Optomechanically enhanced precision measurement

An-Ning Xu[1] and Yong-Chun Liu[1,2,*]

[1]*State Key Laboratory of Low-Dimensional Quantum Physics, Department of Physics, Tsinghua University, Beijing 100084, People's Republic of China*

[2]*Frontier Science Center for Quantum Information, Beijing 100084, People's Republic of China*

(Received 19 February 2022; accepted 28 June 2022; published 12 July 2022)

Cavity optomechanical systems provide excellent platforms for the high-precision measurement of various physical quantities. Here, we investigate the improvement of optomechanical precision measurements based on the tuning of the optomechanical interaction, which can surpass the quantum shot-noise limit without using a squeezed light source. The enhanced performance comes from the optomechanical two-mode squeezing interaction. The approach is based on the tuning of the mechanical susceptibility using optical force, which can be adjusted by controlling the laser frequency and power. For proper blue-detuned laser driving, the mechanical response to the detected signal is greatly enhanced, with improved measurement sensitivity surpassing the shot-noise limit. Moreover, for proper red-detuned laser driving, the working bandwidth can be broadened when the quantum shot noise does not dominate. Our work opens an avenue towards significant improvement to all kinds of optomechanical precision-measurement systems without stringent requirements.

DOI: 10.1103/PhysRevA.106.013506

I. INTRODUCTION

Cavity optomechanics [1–5], which facilitates interactions between optical cavity fields and mechanical resonators, provides an important platform for the manipulation of mechanical resonators in the quantum regime [6–10]. Recently, cavity optomechanical systems have been demonstrated to possess unique advantages in high-precision measurement and sensing, which are able to efficiently transduce various types of physical quantities into displacement with sensitive readout [11–13]. They have been applied to the study of displacement sensing [14–16], mass sensing [17,18], force sensing [19,20], torque sensing [21], acoustic sensing [22–33], atomic force microscopy [34–36], magnetic resonance force microscopy [37–39], accelerometry [40,41], and magnetometry [21,42–49].

Currently, in most of the experiments for precision measurements, the optomechanical interactions are only used to realize the transduction of mechanical displacements into optical signals. As a result, the measurement sensitivities are finally limited by the quantum shot noise of light. Although squeezed light can be used to suppress the quantum shot noise [50–54], it greatly increases the system complexity. In this paper, we analyze the potential of improving the measurement sensitivity by making use of the optomechanical interaction, without the use of the squeezed light source. The enhanced performance comes from the optomechanical two-mode squeezing interaction. By adjusting the laser detuning, the mechanical susceptibility can be tuned freely, leading to the modification of the mechanical response to the detected signal. For blue-detuned laser driving, the response is greatly enhanced, with an improved signal-to-noise ratio (SNR), which surpasses the shot-noise limit. On the other hand, when the quantum shot noise is not the dominant noise source, a red-detuned laser driving leads to the broadening of the working bandwidth.

II. SYSTEM MODEL

A typical optomechanical system consists of an optic cavity and a mechanical resonator. As shown in Fig. 1(a), we consider a basic model of an optomechanical system containing a Fabry-Pérot (FP) cavity with one mirror connected to a spring. The incident laser at frequency $\omega_{\rm L}$ which has a detuning as $\Delta = \omega_{\rm L} - \omega_{\rm c}$ is coupled to the optical cavity with resonance frequency $\omega_{\rm c}$. The intracavity field exerts a radiation-pressure force on the mechanical resonator with effective mass m, mechanical resonance frequency ω_m, and zero-point fluctuation amplitude $x_{\rm ZPF} = \sqrt{\hbar/(2m\omega_{\rm m})}$. Without loss of generality, the physical quantity to be measured is assumed to be an external force F exerted on the mechanical resonator, which can also be replaced by other physical quantities such as acceleration, magnetic field, etc.

The system Hamiltonian [1,55] is given by

$$H = \hbar\omega_{\rm c}a^\dagger a + \hbar\omega_{\rm m}b^\dagger b + \hbar g a^\dagger a(b+b^\dagger) + \hbar(\Omega e^{-i\omega_{\rm L}t}a^\dagger + {\rm H.c.}) - Fx_{\rm ZPF}(b+b^\dagger), \quad (1)$$

where $a^\dagger$ (a) is the photon creation (annihilation) operator, $b^\dagger$ (b) is the phonon creation (annihilation) operator, g is the single-photon optomechanical coupling strength, and Ω is the laser driving strength. When the laser driving is strong so that the intracavity photon number $n_{\rm c} \gg 1$, the system can be linearized with the Hamiltonian simplified as $H_L = -\hbar\Delta a^\dagger a + \hbar\omega_{\rm m}b^\dagger b + \hbar(Ga^\dagger + G^*a)(b+b^\dagger) - Fx_{\rm ZPF}(b+b^\dagger)$, where G

*ycliu@tsinghua.edu.cn

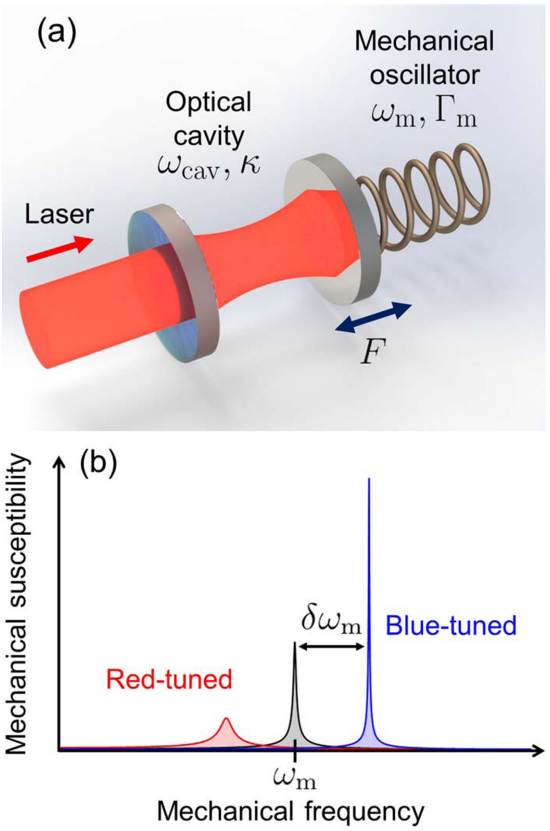

FIG. 1. (a) A typical optomechanical system consists of an optical cavity with one side mirror connected to a mechanical resonator. The optical cavity has a cavity resonance frequency ω_{cav} and a cavity decay rate κ, while the mechanical resonator has a mechanical resonance frequency ω_m and a mechanical damping rate Γ_m. (b) Typical mechanical susceptibilities of the optomechanical system for red-detuned (red curve) and blue-detuned (blue curve) laser inputs. The black curve denotes the bare mechanical susceptibility without an optomechanical interaction.

is the strength of light-enhanced optomechanical coupling. The equation of the motion in the frequency domain reads

$$\frac{\tilde{a}(\omega)}{\chi_c(\omega)} = -iG[\tilde{b}^\dagger(\omega) + \tilde{b}(\omega)] - \sqrt{\kappa}\tilde{a}_{in}(\omega), \tag{2}$$

$$\frac{\tilde{b}(\omega)}{\chi_m(\omega)} = -i[G^*\tilde{a}(\omega) + G\tilde{a}^\dagger(\omega)] + iF\frac{x_{ZPF}}{\hbar} - \sqrt{\Gamma_m}\tilde{b}_{in}(\omega), \tag{3}$$

where $\chi_c(\omega) = (-i\omega - i\Delta + \kappa/2)^{-1}$ and $\chi_m(\omega) = (-i\omega + i\omega_m + \Gamma_m/2)^{-1}$ are the response functions (susceptibilities) of the optical and mechanical modes, and $\kappa = \kappa_0 + \kappa_{ex}$ and Γ_m are the damping rates for the optical and mechanical modes, with the corresponding noise operators being $\tilde{a}_{in}(\omega) = \sqrt{\kappa_0/\kappa}\tilde{a}_{in,0}(\omega) + \sqrt{\kappa_{ex}/\kappa}\tilde{a}_{in,ex}(\omega)$ and $\tilde{b}_{in}(\omega)$, respectively. Here, κ_0 and κ_{ex} are the intrinsic damping rate and the external damping rate from the input coupling, with the noise operators being $\tilde{a}_{in,0}(\omega)$ and $\tilde{a}_{in,ex}(\omega)$, respectively.

Note that the strength of light-enhanced optomechanical coupling $|G| = \sqrt{n_c}g$ depends on the intracavity photon number $n_c = \kappa_{ex}P_{in}/[\hbar\omega_L(\Delta^2 + \kappa^2/4)]$ and the single-photon optomechanical coupling strength $g = x_{ZPF}\partial(\omega_c/\partial x)$. For an FP cavity with length L, we obtain $\partial\omega_c/\partial x = \omega_c/L$, which yields [1]

$$|G| = \frac{\omega_c}{L}\sqrt{\frac{2\kappa_{ex}P_{in}}{m\omega_m\omega_L(4\Delta^2 + \kappa^2)}}, \tag{4}$$

where P_{in} is the input laser power. The argument of G is determined by the incident laser, which can be assumed to be zero without loss of generality, i.e., G is assumed to be real.

From Eqs. (2) and (3) we obtain

$$\frac{\tilde{b}(\omega)}{\chi_m^{eff}(\omega)} \simeq iF\frac{x_{ZPF}}{\hbar} - \sqrt{\Gamma_m}\tilde{b}_{in}(\omega) + i\sqrt{\kappa}[G^*\chi_c(\omega)\tilde{a}_{in}(\omega) + G\chi_c^*(-\omega)\tilde{a}_{in}^\dagger(\omega)]. \tag{5}$$

Here, the effective mechanical susceptibility is given by

$$\chi_m^{eff}(\omega) = \frac{1}{\chi_m^{-1}(\omega) + i\Sigma(\omega)} = \frac{1}{-i\omega + i(\omega_m + \delta\omega_m) + \frac{\Gamma_m + \Gamma_{opt}}{2}}, \tag{6}$$

where $\Sigma(\omega)$ represents the optomechanical self-energy which modifies the mechanical resonance, with the expression given by

$$\Sigma(\omega) = -i|G|^2[\chi_c(\omega) - \chi_c^*(-\omega)] = 2|G|^2\Delta\frac{\Delta^2 + \frac{\kappa^2}{4} - \omega^2 + i\omega\kappa}{\left(\Delta^2 + \frac{\kappa^2}{4} - \omega^2\right)^2 + \omega^2\kappa^2}. \tag{7}$$

The resonance frequency shift $\delta\omega_m$ and the extra damping Γ_{opt} of the mechanical modes are given by

$$\delta\omega_m = \mathrm{Re}\,\Sigma(\omega) = \frac{2|G|^2\Delta\left(\Delta^2 + \frac{\kappa^2}{4} - \omega^2\right)}{\left(\Delta^2 + \frac{\kappa^2}{4} - \omega^2\right)^2 + \omega^2}\kappa^2, \tag{8}$$

$$\Gamma_{opt} = -2\,\mathrm{Im}\,\Sigma(\omega) = \frac{-4|G|^2\Delta\omega\kappa}{\left(\Delta^2 + \frac{\kappa^2}{4} - \omega^2\right)^2 + \omega^2\kappa^2}. \tag{9}$$

III. MECHANICAL RESPONSE

Note that the optomechanical damping rate Γ_{opt} greatly affects the mechanical response. It is shown from Eq. (9) that Γ_{opt} is an odd function with respect to the detuning Δ. For blue-detuned laser driving ($\Delta > 0$), Γ_{opt} is a negative value, corresponding to antidamping, which reduces the total mechanical damping $\Gamma_{eff} = \Gamma_m + \Gamma_{opt}$, leading to the amplification of the mechanical motion, and thereby increasing the response of the system to the signal to be measured [blue curve in Fig. 1(b)]. To keep the system in the stable regime, we require $\Gamma_{opt} > -\Gamma_m$ so that $\Gamma_{eff} > 0$. Oppositely, for red-detuned laser driving ($\Delta < 0$), Γ_{opt} corresponds to additional mechanical damping, which broadens the mechanical response bandwidth [red curve in Fig. 1(b)] [1]. In order to produce a strong antidamping effect with low input laser power, we need to determine the optimal detuning Δ_{max}, which depends on the comparison between the cavity damping rate κ and the mechanical resonance frequency ω_m. In the

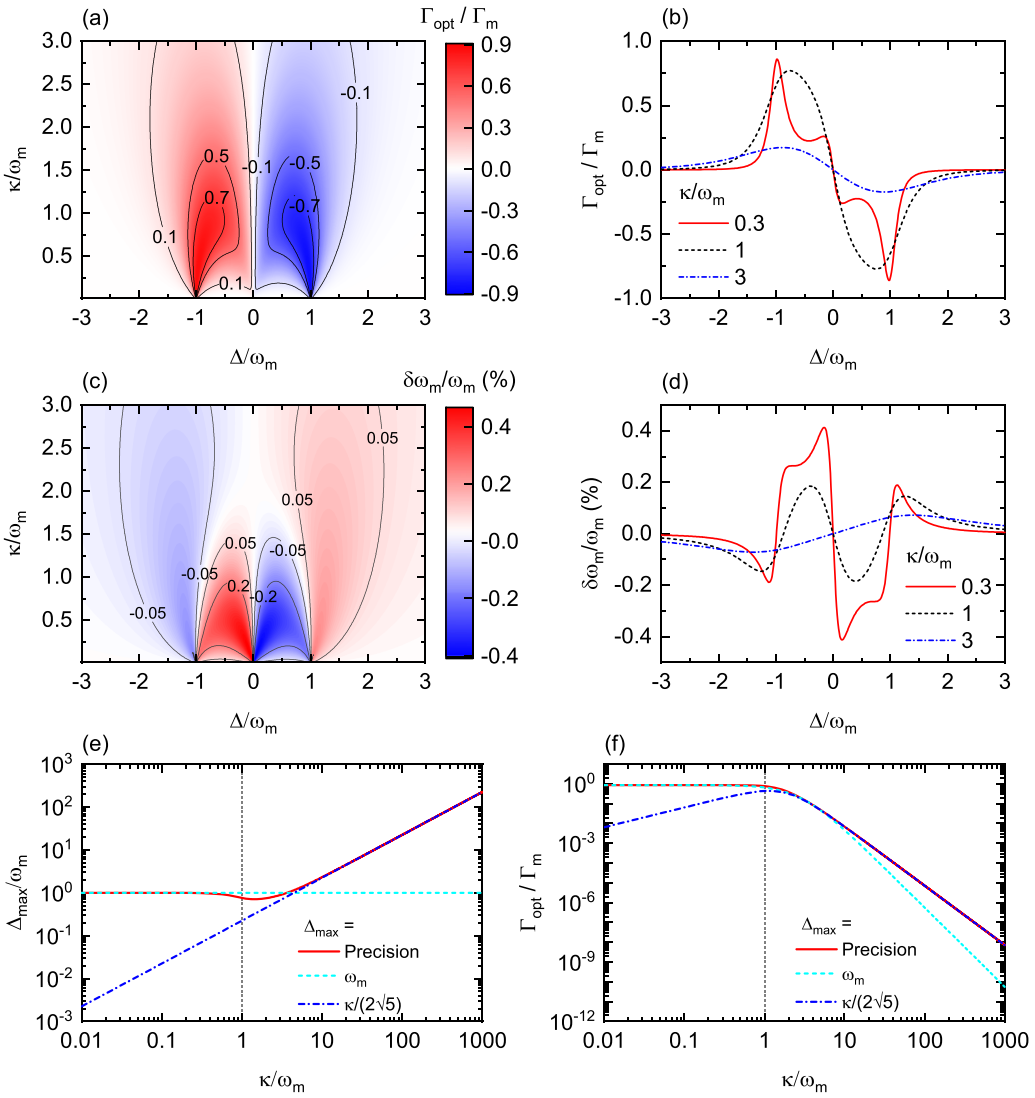

FIG. 2. (a) and (b) The influences on the optomechanical damping rate $\Gamma_{\rm opt}$ from different laser detunings Δ and cavity decay rates κ. (c) and (d) The influences on the mechanical resonance frequency $\omega_{\rm m}$ from different laser detunings Δ and cavity decay rates κ. The red solid, black dashed, and blue dashed-dotted curves in (b) and (d) represent $\kappa/\omega_{\rm m} = 0.3$, 1, and 3, respectively. (e) The optimal laser detuning corresponding to the maximum optomechanical damping rate as a function of $\kappa/\omega_{\rm m}$. The red solid curve corresponds to the exact solution. The cyan dashed curve corresponds to $\Delta_{\rm max} = \omega_{\rm m}$ and the blue dashed-dotted curve corresponds to $\Delta_{\rm max} = \kappa/2\sqrt{5}$. (f) The maximum of the optomechanical damping rate $\Gamma_{\rm opt}$ as a function of $\kappa/\omega_{\rm m}$. Here, we consider a typical SiN membrane mechanical resonator with the mechanical resonance frequency $\omega_{\rm m}/2\pi = 1.6$ MHz, mechanical damping rate $\Gamma_{\rm m}/2\pi = 16$ kHz, cavity length $L = 10$ mm, mass $m = 340$ ng, and the 1550-nm laser incident power $P_{\rm in} = 15$ μW.

resolved-sideband regime ($\kappa \ll \omega_{\rm m}$), we obtain

$$\Delta_{\rm max} = \omega_{\rm m}, \quad \delta\omega_{\rm m} = \frac{|G|^2}{2\omega_{\rm m}}, \quad \Gamma_{\rm opt} = -\frac{4|G|^2}{\kappa}. \tag{10}$$

In the unresolved-sideband regime ($\kappa \gg \omega_{\rm m}$), according to Eqs. (4), (8), and (9), we obtain

$$\Delta_{\rm max} = \frac{\kappa}{2\sqrt{5}}, \quad \delta\omega_{\rm m} = \frac{2\sqrt{5}|G|^2}{3\kappa}, \quad \Gamma_{\rm opt} = -\frac{40\sqrt{5}|G|^2\omega_{\rm m}}{9\kappa^2}. \tag{11}$$

In the opposite case, to produce a strong damping effect, we only need to change the sign in the above expressions.

In Figs. 2(a)–2(d) we plot $\Gamma_{\rm opt}$ and $\delta\omega_{\rm m}$ as functions of the laser detuning Δ and the cavity damping rate κ, which verifies the above analytical expressions. The optimal detuning $\Delta_{\rm max}$ and the corresponding maximum $|\Gamma_{\rm opt}|$ as functions of the cavity damping rate κ are plotted in Figs. 2(e) and 2(f). It reveals that the situations for the resolved and unresolved sideband regimes are quite different. In the resolved-sideband regime, the optimal detuning is fixed around $\Delta_{\rm max} = \omega_{\rm m}$, and the maximum $|\Gamma_{\rm opt}|$ is almost unchanged. In the unresolved-sideband regime, the optimal detuning $\Delta_{\rm max} = \kappa/(2\sqrt{5})$ is proportional to the cavity damping rate κ, while the maximum $|\Gamma_{\rm opt}|$ decreases rapidly as κ increases. The reasons are twofold. On one hand, the increase of the cavity damping rate κ leads to the decrease of the intracavity photon number $n_{\rm c}$, which then degrades the optomechanical coupling strength $|G|$. On the other hand, a large κ greatly broadens

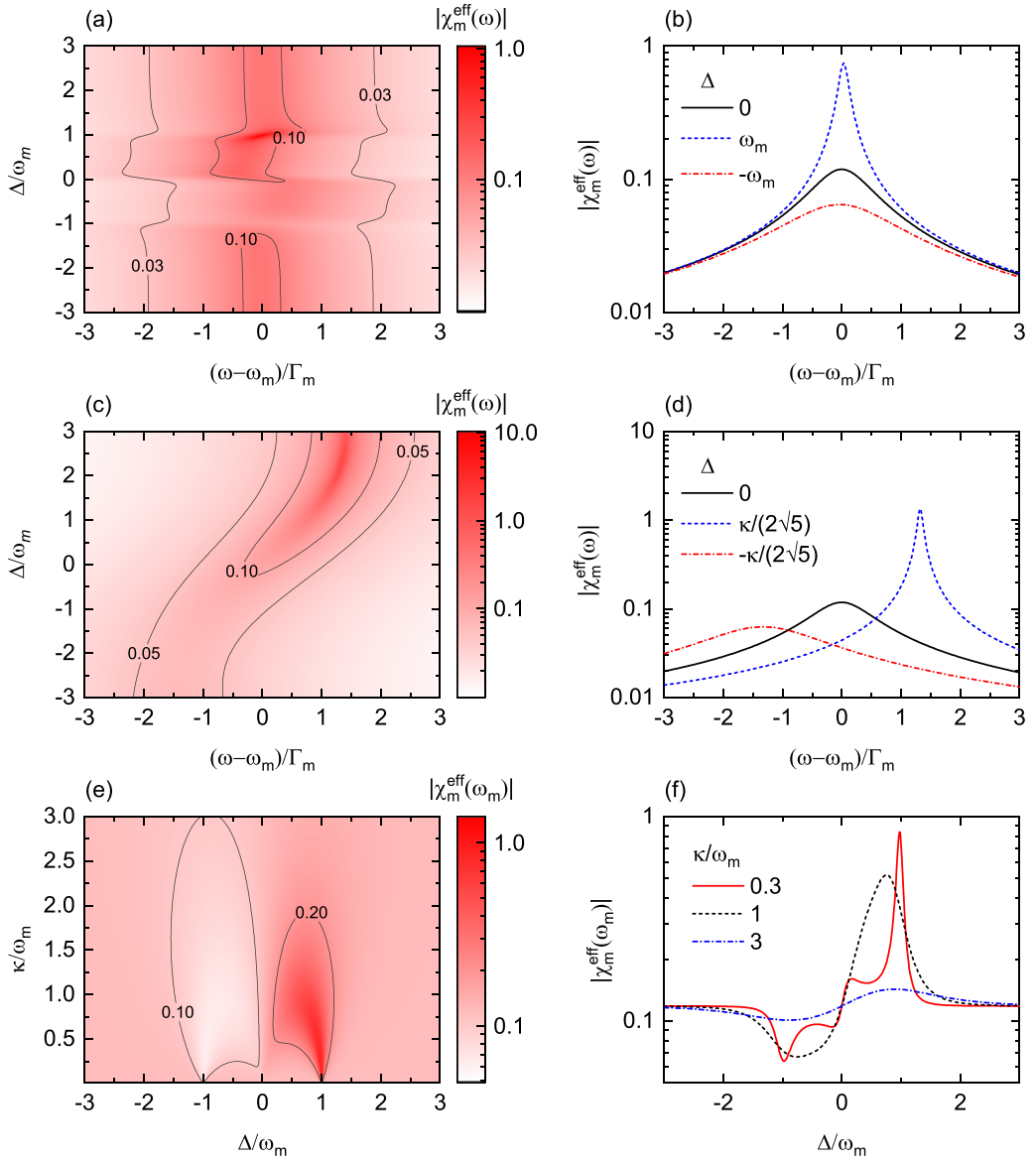

FIG. 3. (a)–(d) The absolute value of effective mechanical susceptibilities for different laser detunings Δ. (a) and (b) are situations in the resolved-sideband regime with $\kappa/\omega_m = 0.3$, while (c) and (d) are in the unresolved-sideband regime with $\kappa/\omega_m = 10$. The blue/black/red curves in (b) and (d) correspond to blue/zero/red detuning of the input lasers with the values shown in the figures, respectively. (e), (f) The peak value of the effective mechanical susceptibilities under different laser detunings and cavity decay rates, with the same input laser power. The red solid line, black dashed, and blue dashed-dotted curves in (f) represent $\kappa/\omega_m = 0.3$, 1, and 3, respectively. The input laser power is $P_{in} = 15\ \mu$W in (a), (b), (e), (f) and $P_{in} = 2$ mW in (c), (d). Other parameters are the same as those in Fig. 2.

the optical response, which strongly mixes the red and blue mechanical sidebands, reducing the net optomechanical damping/antidamping effect. Therefore, in the unresolved-sideband regime, a larger laser power is required to achieve the same optomechanical damping/antidamping effect.

The mechanical susceptibilities $|\chi_m^{eff}(\omega)|$ for different detuning Δ are plotted in Fig. 3. The results in the resolved-sideband regime with $\kappa/\omega_m = 0.3$ are depicted in Figs. 3(a) and 3(b), and the results in the unresolved-sideband regime with $\kappa/\omega_m = 3$ are shown in Figs. 3(c) and 3(d). For a better comparison, the laser powers for the two situations are different to ensure the peak values of the mechanical susceptibilities are comparable. We can find that the mechanical susceptibility strongly increases for blue-detuned driving, while it decreases for red-detuned driving. The shift of the resonance point for the mechanical susceptibility, determined by Eq. (8), is a nonmonotonic function of laser detuning. For the optimal detuning case, the shift can almost be neglected in the resolved-sideband regime, but needs to be considered in the unresolved-sideband regime, as in the latter case the required laser power is larger, and the corresponding mechanical resonance frequency shift becomes notable.

IV. SENSITIVITY ENHANCEMENT

Now we discuss how the measurement sensitivity can be enhanced by considering the noises. From Eqs. (2) and (3) we

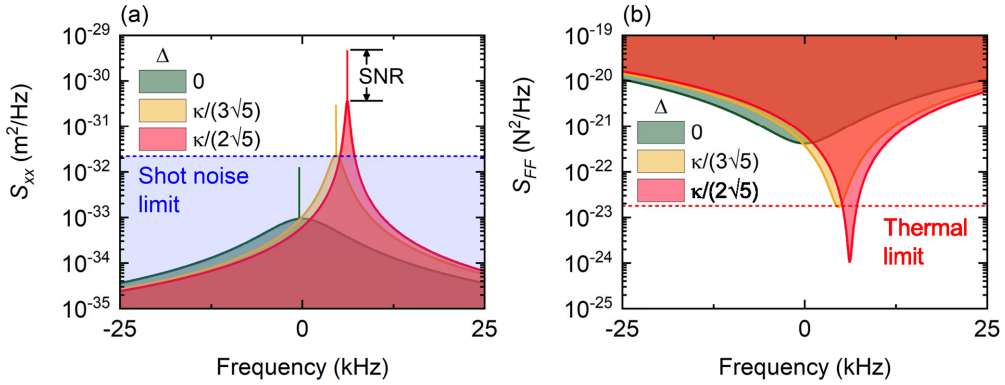

FIG. 4. Optomechanically enhanced precision measurement in a shot-noise-dominant regime. (a) Displacement spectrum densities S_{xx} under different laser detunings as $\Delta = 0, \kappa/(3\sqrt{5}), \kappa/(2\sqrt{5})$, respectively. The blue dashed line is the level of shot noise. (b) The corresponding force spectrum densities S_{FF} with the laser detunings are the same as in (a). The red dashed line is the level of thermal noise. Here, we consider a whispering-gallery-mode cavity [42] with radius $R = 30\ \mu$m, mass $m = 35$ ng, mechanical resonance frequency $\omega_m/2\pi = 10$ MHz, mechanical damping rate $\Gamma_m = 10$ kHz, and cavity decay rate $\kappa/2\pi = 50$ MHz. The input laser power is $P_{in} = 1$ nW.

further obtain

$$\frac{\tilde{a}(\omega)}{\chi_c(\omega)} = G\chi_m^{\rm eff}(\omega)\frac{x_{\rm ZPF}}{\hbar}F + A_{\rm sh}(\omega) + A_{\rm th}(\omega) + A_{\rm rp}(\omega), \quad (12)$$

which includes four terms. The first term proportional to F represents the system response to the signal to be measured, while the other three terms are related to the noise operators, which represent three different kinds of noises. The first noise term $A_{\rm sh}(\omega) = -\sqrt{\kappa}\tilde{a}_{\rm in}(\omega)$ corresponds to the quantum shot noise of the optical field; the second noise term $A_{\rm th}(\omega) = iG\chi_m^{\rm eff}(\omega)\sqrt{\Gamma_m}\tilde{b}_{\rm in}(\omega)$ corresponds to the thermal noise of the mechanical mode, originating from the thermal Brownian movement of the mechanical resonator; the third noise term $A_{\rm rp}(\omega) = G\chi_m^{\rm eff}(\omega)\sqrt{\kappa}[G^*\chi_c(\omega)\tilde{a}_{\rm in}(\omega) + G\chi_c^*(-\omega)\tilde{a}_{\rm in}^\dagger(\omega)]$ corresponds to the radiation-pressure noise, which comes from the noise of the optical force with photon number fluctuations. In real experiments, there are also other technical noises such as laser noises caused by the fluctuations of the laser's phase and amplitude, and the electronic noises induced by the imperfection of electronic devices. From Eq. (12) we can find that the signal term is modified by the optomechanical dampling/antidamping effect with effective susceptibility $\chi_m^{\rm eff}(\omega)$, while the noises are not fully affected by $\chi_m^{\rm eff}(\omega)$. Both the thermal noise and the radiation-pressure noise are affected, but the shot noise is not. In addition, the laser noises and electronic noise will also not be affected by $\chi_m^{\rm eff}(\omega)$. Therefore, changing the effective susceptibility $\chi_m^{\rm eff}(\omega)$ will lead to the change of the SNR, providing the possibility to improve the measurement.

When the system is dominated by the quantum shot noise, we can use a blue-detuned laser input, with a negative $\Gamma_{\rm opt}$ and an increased effective susceptibility $\chi_m^{\rm eff}(\omega)$. Then the signal response increases, while the main noise remains unchanged. Thus, the SNR becomes larger, and the shot noise will no longer be the limiting factor. The optomechanical antidamping effect also amplifies the thermal noise and the radiation-pressure noise, so the final measurement sensitivity will be determined by these two noises. In Fig. 4(a) we take an unresolved-sideband optomechanical system as an example, and plot typical displacement noise spectrum densities $S_{xx}(\omega)$ for different detuning Δ. Originally the system mainly suffers from the shot noise, corresponding to the blue dashed

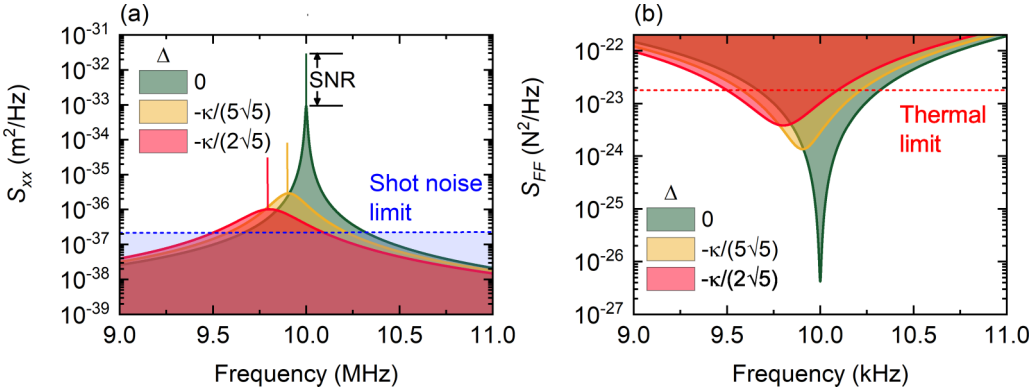

FIG. 5. Optomechanically enhanced precision measurement in a thermal-noise-dominant regime. (a) Displacement spectrum densities S_{xx} under different laser detunings as $\Delta = 0, -\kappa/(5\sqrt{5}), -\kappa/(2\sqrt{5})$, respectively. The blue dashed line is the level of shot noise. (b) The corresponding force spectrum densities S_{FF} with the laser detunings are the same as in (a). The red dashed line is the level of thermal noise. The input laser power is $P_{in} = 0.1$ mW. Other parameters are the same as those in Fig. 4.

horizontal line, which strongly overwhelmed the signal. With the help of optomechanical antidamping, the signal becomes amplified, which then can be extracted from the shot-noise background. When the peak thermal noise reaches the same as the shot-noise level, the increase of the SNR reaches the maximum. The corresponding force noise spectra densities $S_{FF}(\omega)$ are plotted in Fig. 4(b), which clearly shows the final reachable measurement sensitivity. In this case, the measurement sensitivity can reach the thermal noise limit denoted by the red dashed horizontal curve.

In the opposite case, if the system is dominantly limited by the thermal noise (or radiation-pressure noise), then the increase of the effective susceptibility $\chi_{\rm m}^{\rm eff}(\omega)$ no longer improves the SNR. However, we can use a red-detuned laser input, with a positive $\Gamma_{\rm opt}$, to broaden the working bandwidth, which can be increased from $\Gamma_{\rm m}$ to $\Gamma_{\rm m}+\Gamma_{\rm opt}$. In Fig. 5(a) we plot the displacement noise spectrum densities $S_{xx}(\omega)$ and the force noise spectra densities $S_{FF}(\omega)$ for this situation. It shows that the optomechanical damping effect helps to enlarge the bandwidth and the SNR remains unchanged until the peak thermal noise becomes comparable with the shot noise.

V. CONCLUSION

In summary, we study the precision measurement enhanced by manipulating the optomechanical interaction, which can surpass the quantum shot-noise limit, without the use of a squeezed light source. The enhanced performance comes from the optomechanical two-mode squeezing interaction. It only requires the tuning of the frequency and power of the incident laser, which modifies the mechanical susceptibility induced by the optical force. When the system is dominated by the quantum shot noise or classical technical noises, by using blue-detuned laser driving, the signal response is greatly enhanced, with improved measurement sensitivity. When the thermal noise or radiation-pressure noise dominates, by using red-detuned laser driving, the working bandwidth can be broadened. Analytical expressions for the optimal laser detunings for both the resolved-sideband regime and the unresolved-sideband regime are present. Our work provides a promising approach for improving the performance of optomechanical sensors.

ACKNOWLEDGMENTS

This work is supported by the Key-Area Research and Development Program of Guangdong Province (Grant No. 2019B030330001), the National Natural Science Foundation of China (NSFC) (Grants No. 92050110, No. 91736106, No. 11674390, and No. 91836302), and the National Key Research and Development Program of China (Grant No. 2018YFA0306504).

APPENDIX: NOISE ANALYSIS AND DEVIATION

From Eq. (12), we are able to classify the noise into three major resources, which are the quantum shot noise (measurement imprecision noise) due to the fluctuation of the photon number in the cavity, the thermal noise due to the Brownian movement of the mechanical resonator, and the backaction noise due to the radiation pressure from the laser on the resonator. The displacement spectral density S_{xx} is defined as

$$S_{xx}(\omega)=\int_{-\infty}^{\infty}d\omega'\langle\hat{x}^{\dagger}(\omega)\hat{x}(\omega')\rangle, \tag{A1}$$

and the force spectral density S_{FF} defined with $x(\omega)=\chi_{\rm M}(\omega)F(\omega)$ is

$$S_{FF}(\omega)=\frac{S_{xx}(\omega)}{|\chi_{\rm M}(\omega)|^2}. \tag{A2}$$

Here, S_{xx} is proportional to the power spectral density (PSD) on the spectral analyzer because the measurement result is typically proportional to the displacement, while S_{FF} is associated with the physical parameters that are usually measured, including force, torque, mass, acceleration, supersonic wave, magnetic field, etc. According to the definition of the displacement operator $\hat{x}=x_{\rm ZPF}(\hat{b}+\hat{b}^{\dagger})$, we have the displacement operator as

$$\begin{aligned}\frac{\hat{x}}{x_{\rm ZPF}}=&\,iF\frac{x_{\rm ZPF}}{\hbar}\left[\chi_{\rm m}^{\rm eff}(\omega)-\chi_{\rm m}^{\rm eff\,*}(-\omega)\right]\\&-\sqrt{\Gamma_{\rm m}}\left[\chi_{\rm m}^{\rm eff}(\omega)\tilde{b}_{\rm in}+{\rm H.c.}\right]\\&+i\sqrt{\kappa}[G^{*}\chi_{\rm c}(\omega)\tilde{a}_{\rm in}+{\rm H.c.}]\left[\chi_{\rm m}^{\rm eff}(\omega)-\chi_{\rm m}^{\rm eff\,*}(-\omega)\right].\end{aligned} \tag{A3}$$

The noise correlators associated with the input fluctuations are given by

$$\langle a_{{\rm in},0({\rm ex})}(t)a_{{\rm in},0({\rm ex})}^{\dagger}(t')\rangle=\delta(t-t'), \tag{A4}$$

$$\langle a_{{\rm in},0({\rm ex})}^{\dagger}(t)a_{{\rm in},0({\rm ex})}(t')\rangle=0, \tag{A5}$$

$$\langle b_{\rm in}(t)b_{\rm in}^{\dagger}(t')\rangle=(\bar{n}_{\rm th}+1)\delta(t-t'), \tag{A6}$$

$$\langle b_{\rm in}^{\dagger}(t)b_{\rm in}(t')\rangle=\bar{n}_{\rm th}\delta(t-t'), \tag{A7}$$

and the relationships in the frequency domain found by Fourier transformation are

$$\langle a_{{\rm in},0({\rm ex})}(\omega)a_{{\rm in},0({\rm ex})}^{\dagger}(\omega')\rangle=\delta(\omega+\omega'), \tag{A8}$$

$$\langle a_{{\rm in},0({\rm ex})}^{\dagger}(\omega)a_{{\rm in},0({\rm ex})}(\omega')\rangle=0, \tag{A9}$$

$$\langle b_{\rm in}(\omega)b_{\rm in}^{\dagger}(\omega')\rangle=(\bar{n}_{\rm th}+1)\delta(\omega+\omega'), \tag{A10}$$

$$\langle b_{\rm in}^{\dagger}(\omega)b_{\rm in}(\omega')\rangle=\bar{n}_{\rm th}\delta(\omega+\omega'). \tag{A11}$$

Here, $\bar{n}_{\rm th}=[\exp(\hbar\omega_{\rm m}/k_BT)-1]^{-1}$ is the average thermal phonon number under thermal equilibrium. Therefore, we obtain the displacement spectral density as

$$\begin{aligned}S_{xx}(\omega)=&\,x_{\rm ZPF}^2\Gamma_{\rm m}\left[\bar{n}_{\rm th}\left|\chi_{\rm m}^{\rm eff\,*}(-\omega)\right|^2+(\bar{n}_{\rm th}+1)\left|\chi_{\rm m}^{\rm eff}(\omega)\right|^2\right]\\&+x_{\rm ZPF}^2\kappa\left|\chi_{\rm m}^{\rm eff\,*}(-\omega)-\chi_{\rm m}^{\rm eff}(\omega)\right|^2|G|^2|\chi_{\rm c}(\omega)|^2.\end{aligned} \tag{A12}$$

The first term describes the thermal noise and the second term describes the backaction noise. We are able to get the force

spectral density as

$$S_{FF}^{\mathrm{th}} \simeq 2mk_BT\omega_{\mathrm{m}}, \tag{A13}$$

$$S_{FF}^{\mathrm{rp}} = \frac{\kappa\hbar^2}{x_{\mathrm{ZPF}}^2}|G|^2|\chi_{\mathrm{c}}(\omega)|^2. \tag{A14}$$

Now we turn our attention to the imprecision of the measurement due to shot noise in the output. The appropriate homodyne quadrature variable to monitor to be sensitive to the output phase shift caused by position fluctuations is

$$I = a_{\mathrm{out}} + a_{\mathrm{out}}^{\dagger}. \tag{A15}$$

According to the input-output theory of open quantum systems, the field that is reflected from the cavity is given by

$$a_{\mathrm{out}} = a_{\mathrm{in}} - \sqrt{\kappa_{\mathrm{ex}}}a. \tag{A16}$$

Thus the measurement imprecision spectral density referred back to the position of the mechanical resonator is

$$S_{xx}^{\mathrm{sh}} = \frac{1}{4\kappa_{\mathrm{ex}}}\frac{x_{\mathrm{ZPF}}^2}{|G|^2|\chi_{\mathrm{c}}(\omega)|^2}. \tag{A17}$$

Comparing this to Eq. (A4) we see that we reach the quantum limit relating the imprecision noise to backaction noise

$$S_{xx}^{\mathrm{sh}}S_{FF}^{\mathrm{rp}} = \frac{\hbar^2}{4}\frac{\kappa}{\kappa_{\mathrm{ex}}} = \frac{\hbar^2}{4\eta_{\mathrm{c}}} \geqslant \frac{\hbar^2}{4}, \tag{A18}$$

where $\eta_{\mathrm{c}} = \kappa_{\mathrm{ex}}/\kappa$ is the coupling efficiency of the cavity. For a mechanical resonator possessing a larger quality factor ($\omega_{\mathrm{m}} \gg \Gamma_{\mathrm{m}}$), the displacement spectral density can be described as

$$S_{xx}^{\mathrm{tot}}(\omega) = S_{xx}^{\mathrm{sh}}(\omega) + |\chi_{\mathrm{M}}(\omega)|^2\left[S_{FF}^{\mathrm{th}} + S_{FF}^{\mathrm{rp}}(\omega)\right]. \tag{A19}$$

With this equation, we are able to obtain the total noise displacement power density of the system.

[1] M. Aspelmeyer, T. J. Kippenberg, and F. Marquardt, Rev. Mod. Phys. **86**, 1391 (2014).

[2] W. P. Bowen and G. J. Milburn, *Quantum Optomechanics* (CRC Press, Boca Raton, FL, 2015).

[3] T. J. Kippenberg and K. J. Vahala, Opt. Express **15**, 17172 (2007).

[4] T. J. Kippenberg and K. J. Vahala, Science **321**, 1172 (2008).

[5] P. Meystre, Ann. Phys. **525**, 215 (2013).

[6] A. Schliesser, R. Rivière, G. Anetsberger, O. Arcizet, and T. J. Kippenberg, Nat. Phys. **4**, 415 (2008).

[7] A. Schliesser, O. Arcizet, R. Rivière, G. Anetsberger, and T. J. Kippenberg, Nat. Phys. **5**, 509 (2009).

[8] A. D. O'Connell, M. Hofheinz, M. Ansmann, R. C. Bialczak, M. Lenander, E. Lucero, M. Neeley, D. Sank, H. Wang, M. Weides, J. Wenner, J. M. Martinis, and A. N. Cleland, Nature (London) **464**, 697 (2010).

[9] J. Chan, T. P. M. Alegre, A. H. Safavi-Naeini, J. T. Hill, A. Krause, S. Gröblacher, M. Aspelmeyer, and O. Painter, Nature (London) **478**, 89 (2011).

[10] J. D. Teufel, T. Donner, D. Li, J. W. Harlow, M. S. Allman, K. Cicak, A. J. Sirois, J. D. Whittaker, K. W. Lehnert, and R. W. Simmonds, Nature (London) **475**, 359 (2011).

[11] Y.-W. Hu, Y.-F. Xiao, Y.-C. Liu, and Q. Gong, Front. Phys. **8**, 475 (2013).

[12] M. Metcalfe, Appl. Phys. Rev. **1**, 031105 (2014).

[13] B.-B. Li, L. Ou, Y. Lei, and Y.-C. Liu, Nanophotonics **10**, 2799 (2021).

[14] G. Anetsberger, O. Arcizet, Q. P. Unterreithmeier, R. Rivière, A. Schliesser, E. M. Weig, J. P. Kotthaus, and T. J. Kippenberg, Nat. Phys. **5**, 909 (2009).

[15] A. Schliesser, G. Anetsberger, R. Rivière, O. Arcizet, and T. J. Kippenberg, New J. Phys. **10**, 095015 (2008).

[16] G. Anetsberger, E. Gavartin, O. Arcizet, Q. P. Unterreithmeier, E. M. Weig, M. L. Gorodetsky, J. P. Kotthaus, and T. J. Kippenberg, Phys. Rev. A **82**, 061804(R) (2010).

[17] F. Liu, S. Alaie, Z. C. Leseman, and M. Hossein-Zadeh, Opt. Express **21**, 19555 (2013).

[18] J.-J. Li and K.-D. Zhu, Phys. Rep. **525**, 223 (2013).

[19] E. Gavartin, P. Verlot, and T. J. Kippenberg, Nat. Nanotechnol. **7**, 509 (2012).

[20] I. D. Stoev, B. Seelbinder, E. Erben, N. Maghelli, and M. Kreysing, eLight **1**, 7 (2021).

[21] M. Wu, N. L. Y. Wu, T. Firdous, F. Fani Sani, J. E. Losby, M. R. Freeman, and P. E. Barclay, Nat. Nanotechnol. **12**, 127 (2017).

[22] S. Basiri-Esfahani, A. Armin, S. Forstner, and W. P. Bowen, Nat. Commun. **10**, 132 (2019).

[23] F. Monifi, B. Peng, Ş. K. Özdemir, L. Ma, K. Maslov, L. V. Wang, and L. Yang, in *2013 IEEE Photonics Conference* (IEEE, New York, 2013), pp. 215–216.

[24] M. V. Chistiakova and A. M. Armani, Opt. Express **22**, 28169 (2014).

[25] K. H. Kim, W. Luo, C. Zhang, C. Tian, L. J. Guo, X. Wang, and X. Fan, Sci. Rep. **7**, 109 (2017).

[26] J. Pan, B. Zhang, Z. Liu, J. Zhao, Y. Feng, L. Wan, and Z. Li, Photonics Res. **8**, 303 (2020).

[27] J. A. Guggenheim, J. Li, T. J. Allen, R. J. Colchester, S. Noimark, O. Ogunlade, I. P. Parkin, I. Papakonstantinou, A. E. Desjardins, E. Z. Zhang, and P. C. Beard, Nat. Photonics **11**, 714 (2017).

[28] C. Zhang, T. Ling, S.-L. Chen, and L. J. Guo, ACS Photonics **1**, 1093 (2014).

[29] H. Li, B. Dong, Z. Zhang, H. F. Zhang, and C. Sun, Sci. Rep. **4**, 4496 (2014).

[30] H. Li, B. Dong, X. Zhang, X. Shu, X. Chen, R. Hai, D. A. Czaplewski, H. F. Zhang, and C. Sun, Nat. Commun. **10**, 4277 (2019).

[31] J. Yang, T. Qin, F. Zhang, X. Chen, X. Jiang, and W. Wan, Nanophotonics **9**, 176 (2020).

[32] R. Shnaiderman, G. Wissmeyer, O. Ülgen, Q. Mustafa, A. Chmyrov, and V. Ntziachristos, Nature (London) **585**, 372 (2020).

[33] W. J. Westerveld, M. Mahmud-Ul-Hasan, R. Shnaiderman, V. Ntziachristos, X. Rottenberg, S. Severi, and V. Rochus, Nat. Photonics **15**, 341 (2021).

[34] K. Srinivasan, H. Miao, M. T. Rakher, M. Davanço, and V. Aksyuk, Nano Lett. **11**, 791 (2011).

[35] J. Chae, S. An, G. Ramer, V. Stavila, G. Holland, Y. Yoon, A. A. Talin, M. Allendorf, V. A. Aksyuk, and A. Centrone, Nano Lett. **17**, 5587 (2017).
[36] P. E. Allain, L. Schwab, C. Mismer, M. Gely, E. Mairiaux, M. Hermouet, B. Walter, G. Leo, S. Hentz, M. Faucher, G. Jourdan, B. Legrand, and I. Favero, Nanoscale **12**, 2939 (2020).
[37] H. J. Mamin, R. Budakian, B. W. Chui, and D. Rugar, Phys. Rev. Lett. **91**, 207604 (2003).
[38] D. Rugar, R. Budakian, H. J. Mamin, and B. W. Chui, Nature (London) **430**, 329 (2004).
[39] R. Fischer, D. P. McNally, C. Reetz, G. G. T. Assumpção, T. Knief, Y. Lin, and C. A. Regal, New J. Phys. **21**, 043049 (2019).
[40] A. G. Krause, M. Winger, T. D. Blasius, Q. Lin, and O. Painter, Nat. Photonics **6**, 768 (2012).
[41] F. Guzmán Cervantes, L. Kumanchik, J. Pratt, and J. M. Taylor, Appl. Phys. Lett. **104**, 221111 (2014).
[42] S. Forstner, S. Prams, J. Knittel, E. D. van Ooijen, J. D. Swaim, G. I. Harris, A. Szorkovszky, W. P. Bowen, and H. Rubinsztein-Dunlop, Phys. Rev. Lett. **108**, 120801 (2012).
[43] S. Forstner, E. Sheridan, J. Knittel, C. L. Humphreys, G. A. Brawley, H. Rubinsztein, and W. P. Bowen, Adv. Mater. **26**, 6348 (2014).
[44] W. Yu, W. C. Jiang, Q. Lin, and T. Lu, Nat. Commun. **7**, 12311 (2016).
[45] B.-B. Li, D. Bulla, V. Prakash, S. Forstner, A. Dehghan-Manshadi, H. Rubinsztein-Dunlop, S. Foster, and W. P. Bowen, APL Photonics **3**, 120806 (2018).
[46] B.-B. Li, G. Brawley, H. Greenall, S. Forstner, E. Sheridan, H. Rubinsztein-Dunlop, and W. P. Bowen, Photonics Res. **8**, 1064 (2020).
[47] J. Zhu, G. Zhao, I. Savukov, and L. Yang, Sci. Rep. **7**, 8896 (2017).
[48] E. Freeman, C.-Y. Wang, V. Sumaria, S. J. Schiff, Z. Liu, and S. Tadigadapa, AIP Adv. **8**, 065214 (2018).
[49] M. F. Colombano, G. Arregui, F. Bonell, N. E. Capuj, E. Chavez-Angel, A. Pitanti, S. O. Valenzuela, C. M. Sotomayor-Torres, D. Navarro-Urrios, and M. V. Costache, Phys. Rev. Lett. **125**, 147201 (2020).
[50] B.-B. Li, J. Bílek, U. B. Hoff, L. S. Madsen, S. Forstner, V. Prakash, C. Schäfermeier, T. Gehring, W. P. Bowen, and U. L. Andersen, Optica **5**, 850 (2018).
[51] J. Aasi, J. Abadie, B. P. Abbott, R. Abbott, T. D. Abbott, M. R. Abernathy, and Adams, Nat. Photonics **7**, 613 (2013).
[52] U. B. Hoff, G. I. Harris, L. S. Madsen, H. Kerdoncuff, M. Lassen, B. M. Nielsen, W. P. Bowen, and U. L. Andersen, Opt. Lett. **38**, 1413 (2013).
[53] R. C. Pooser and B. Lawrie, Optica **2**, 393 (2015).
[54] B. J. Lawrie, P. D. Lett, A. M. Marino, and R. C. Pooser, ACS Photonics **6**, 1307 (2019).
[55] Y.-C. Liu, Y.-W. Hu, C. W. Wong, and Y.-F. Xiao, Chin. Phys. B **22**, 114213 (2013).